Atmos. Chem. Phys., 26, 14471–14485, 2026
https://doi.org/10.5194/acp-26-14471-2026
© Author(s) 2026. This work is distributed under
the Creative Commons Attribution 4.0 License.

Atmospheric Chemistry and Physics
Open Access
EGU

Research article

Sensitivity of the summertime diurnal precipitation cycle over three representative regions of China to convective trigger and closure treatments in a single-column model

Xiaocong Wang[1], **Yanjie Liu**[1,2], **and Yimin Liu**[1,2]

[1]Institute of Atmospheric Physics (IAP), Chinese Academy of Sciences (CAS), Beijing, China
[2]College of Earth and Planetary Sciences, University of Chinese Academy of Sciences (UCAS), Beijing, China

Correspondence: Xiaocong Wang (wangxc@lasg.iap.ac.cn)

Received: 6 July 2026 – Discussion started: 15 July 2026
Revised: 18 September 2026 – Accepted: 4 October 2026 – Published: 13 October 2026

Abstract. Using a single-column model, we investigate how trigger and closure treatments in ZM, TDK, and UNICON convection schemes affect the diurnal cycle of precipitation over China. For late-afternoon rainfall, TDK and ZM schemes with standard CAPE closure simulate precipitation peaks around noon, substantially earlier than observed. The UNICON scheme, with cold-pool feedback deactivated, also produces a noontime peak. For nocturnal rainfall, all schemes spuriously produce a noontime peak, in stark contrast to the observed nocturnal maximum. These behaviors are closely related to closure assumptions and the resulting cloud-base mass flux, which is primarily governed by CAPE in ZM and TDK, and responds more directly to surface fluxes in UNICON. By accounting for the imbalance between deep convection and boundary-layer production through specific modifications: adopting the dCAPE trigger in ZM, activating cold-pool feedback in UNICON, and applying the non-equilibrium closure in TDK, the simulated afternoon precipitation is delayed and in better agreement with observations. In addition, allowing elevated convection in ZM and UNICON improves nocturnal rainfall. The improved diurnal cycle is also evident in the diabatic heating fields. All modifications lead to a delayed and more pronounced upward-tilting heating structure as a result of the suppression of early-afternoon convection, with ZM and TDK extending to higher altitudes, while both intensified and extended in UNICON. These changes alleviate the upper-level cold bias in TDK and ZM. In UNICON, however, the overly strong convection reverses the upper-tropospheric bias from cold to warm with stronger magnitude, thereby worsening the bias.

1 Introduction

The diurnal cycle of precipitation (DCP), which plays a critical role in modulating the surface energy budget and hydrology, has long been recognized as a fundamental mode of variability in the climate system (Trenberth et al., 2003). In addition, DCP also acts as a building block for the large-scale organization of precipitation systems, including convectively coupled equatorial waves and the Madden–Julian Oscillation (Mapes et al., 2006). Therefore, accurate simulation of DCP is not only essential for advancing the precision of "timing–location–intensity" in fine-scale forecasting (Dai and Trenberth, 2004; Chen et al., 2017), but also important for improving processes across a range of temporal and spatial scales – from convective systems to intraseasonal disturbances (Benedict et al., 2013). Nevertheless, DCP modeling in general circulation models (GCMs) remains a persistent challenge, as evidenced by a premature afternoon peak over land and a frequent inability to capture nocturnal rainfall maxima downwind of major orography (Dai, 2006; Lee et al., 2007; Tang et al., 2022).

Over land, the observed DCP typically peaks in late afternoon during summer, partly due to the strong diurnal cycle of surface heat flux that modulates convection (Dai et al.,

1999; Li et al., 2008). However, on the leeside of mountainous regions such as the Tibetan Plateau and the Rockies, the maximum precipitation is often observed in late night, owing to the propagation of mesoscale convective systems induced by terrain-forced circulations (Carbone and Tuttle, 2008; Zhang et al., 2014). Because DCP is closely related to changes in surface temperature and boundary-layer structure on much shorter timescales, it poses a fundamental challenge to the equilibrium assumption commonly used in convection parameterizations (Davies et al., 2013). In this sense, DCP provides a measure of how well a GCM represents the response of cumulus convection to large-scale and surface forcing. Many schemes initiate convection based on convective available potential energy (CAPE), which responds rapidly to solar heating, resulting in overly frequent and premature triggering of afternoon convection (e.g., Xie and Zhang, 2000; Lee et al., 2007; Yang et al., 2018). On the other hand, the failure to capture nocturnal precipitation is often attributed to the inadequate representation of elevated convection originating above the boundary layer. (Lee et al., 2008; Wang et al., 2015; Xie et al., 2019). To overcome these deficiencies, increasing efforts have been devoted to developing improved trigger and closure treatments. For example, Xie and Zhang (2000) proposed dynamic CAPE (dCAPE) triggering, which initializes convection only when the large-scale CAPE production exceeds a critical value. Bechtold et al. (2014) accounted for CAPE consumption by shallow convection and modified the closure to subtract its contribution from the total mass flux. Park (2014a) incorporated subgrid mesoscale organized flow and its feedback into the convection parameterization, enabling the successful simulation of various convection-related transitional phenomena including DCP. To better simulate nocturnal rainfall, Wang et al. (2015) allows parcels to be initiated from above the boundary layer, thereby improving the simulation of elevated nocturnal convection over the central Great Plains. This triggering concept was later used in Xie et al. (2019) and Park et al. (2024). While these modifications have mitigated certain DCP biases at the testing sites, it remains unclear how well they generalize to regions with markedly different climatic and topographic conditions, such as China. The present study is therefore motivated to assess their effectiveness of DCP simulation over China. Additionally, despite the documented improvements in DCP simulation achieved by various approaches, a systematic intercomparison of their performance and underlying mechanisms has yet to be conducted. Liu et al. (2026) performed a process-oriented analysis that traces DCP errors over China in three reanalyses to specific parameterized physical processes, highlighting the critical role of convective trigger in shaping DCP. This study builds on Liu et al. (2026) by using a single-column model (SCM) to further explore the sensitivity of DCP to modifications in convective trigger and closure treatments. Specifically, we assess how precipitation varies diurnally under different trigger and closure treatments, aiming to elucidate the physical mechanisms behind. The remainder of this paper is structured as follows. Section 2 describes the case setup, model configurations, and experimental design. Section 3 presents modifications to the convection schemes and examines the DCP sensitivity to different parameterization settings, along with the underlying mechanisms. Section 4 analyzes the diurnal variations of diabatic heating and convective eddy transport of moist static energy (MSE). Section 5 discusses the implications for temperature and moisture simulations, and Sect. 6 summarizes the main findings.

2 Case, Model and Experiments

2.1 Case Description

The three representative regions used in this study are $4° \times 4°$ subregions of those in Liu et al. (2026): the Tibetan Plateau (TP, 31–35° N, 90–94° E), southeastern China (SECN, 24–28° N, 112–116° E), and the Sichuan Basin (SCB, 28–32° N, 103–107° E). Among these, TP and SECN are characterized by late-afternoon rainfall regimes, while SCB features a nocturnal regime. For each region, DCP is simulated and analyzed over the summer from 1 June–31 August 2021. The initial and large-scale forcing fields used to drive SCMs are derived from ERA5 reanalysis (Hersbach et al., 2020), facilitated by the open-source Python package named the "Large-eddy simulation and Single-column model – Large-Scale Dynamics" (van Stratum et al., 2023). Note that although ERA5 remains one of the most reliable reanalyses, it carries inherent uncertainties. However, considering that this study focuses on the sensitivity of different trigger and closure treatments in influencing DCP, ERA5 forcing suffices for this purpose.

2.2 Model and Experimental Design

We use the single column version of the Community Atmospheric Model (CAM) for SCM simulations, which features a suite of parameterization schemes for cumulus convection (Gettelman et al., 2019). In this study, three distinct configurations are compared: CAM_ZM, CAM_UNICON, and CAM_TDK. In the CAM_ZM setup, deep convection is parameterized using the Zhang and McFarlane (1995) scheme, whereas shallow convection is treated with the Park and Bretherton (2009) scheme. CAM_UNICON employs a unified framework for both shallow and deep convection (Park, 2014a). In addition to ZM and UNICON, the bulk mass-flux scheme originally proposed by Tiedtke (1989; hereafter referred to as TDK) and later updated by Bechtold et al. (2014) was also implemented for comparison, referred to as CAM_TDK. Other parameterizations are set the same across all configurations. The parameterization of planetary boundary layer (PBL) turbulence is according to Bretherton and Park (2009).Cloud microphysics is represented by the double moment scheme of Morrison and Gettelman (2008). Ra-

diative transfer is calculated with the Rapid Radiative Transfer Model for GCMs (Clough et al., 2005). For each convection scheme, two simulations are conducted: a control experiment (CTRL) and a sensitivity experiment (SENS). For CAM_ZM, the sensitivity experiment adopts the dCAPE trigger of Xie and Zhang (2000) and permits elevated convection as in Xie et al. (2019). In CAM_UNICON, the control experiment disables cold-pool feedback, whereas the sensitivity experiment activates cold-pool feedback and allows elevated convection as described in Park et al. (2024). For CAM_TDK, the control experiment employs the equilibrium closure, while the sensitivity experiment applies the non-equilibrium closure as proposed by Bechtold et al. (2014). Table 1 summarizes the key differences in parameterization components across various configurations. To reduce model error accumulation, all simulations are reinitialized daily at 00 UTC from 1 June–31 August and integrated for 36 h without relaxation. The last 24 h of each 36 h simulation are retained for analysis.

2.3 Composite Analysis

To isolate the typical DCP behavior, we performed a composite analysis by selecting precipitation events that represent the characteristic DCP category for each region. Following Liu et al. (2026), we selected afternoon-peaking (12:00–20:00 LST, local solar time) days for TP and SECN, and nocturnal-peaking (20:00–08:00 LST) days for SCB. We also required the daily maximum precipitation to exceed thresholds of 5 mm d^{-1} for TP and 10 mm d^{-1} for SECN and SCB, consistent with those used by Liu et al. (2026). By doing so, the influence of dry days, light precipitation, and days with diurnal phases inconsistent with the target regime is excluded, thereby enhancing the DCP signal. Unlike Liu et al. (2026) that used different event dates across the datasets, we used the same fixed event dates derived from precipitation observations for all model simulations. Although only one summer (2021) is used, this season still provides a sufficient number of precipitation events for robust composite analysis: 49 d over TP, 45 over SECN, and 34 over SCB. These sample sizes are comparable to those used in the observational composites of Liu et al. (2026).

3 Sensitivity of Diurnal Precipitation to Convection Schemes

3.1 Diurnal Precipitation in the Control Experiments

Figure 1 presents the period-averaged and case-composite diurnal variations of precipitation over the three regions from the control experiment. The observation is the Integrated Multi-satellitE Retrievals for Global Precipitation Measurement (IMERG) Final Run Version 07B (Huffman et al., 2023), with ERA5 precipitation also superimposed for reference. A comparison between the upper and middle rows reveals that the composite cycles align closely with the period-mean in phase, and the diurnal signals are amplified due to the removal of light-precipitation days. Over TP and SECN, the IMERG precipitation peaks around 18:00 LST, whereas all simulations produce rainfall peaks notably earlier than observed, with the maximum occurring near noon. In comparison, the ZM and TDK schemes initiate rainfall even earlier than UNICON and tend to produce a secondary peak over SECN – at 19:00 LST for ZM and at 17:00 LST for TDK. Note that ERA5 also exhibits an early phase bias over TP and SECN relative to IMERG, though less pronounced than the SCM simulations. The convective precipitation shown in the bottom closely resembles the total precipitation, suggesting that deficiencies in convection parameterization are largely responsible for the poor simulation of DCP. Over SCB, the observed precipitation exhibits a distinct nocturnal maximum around 03:00 LST, in stark contrast to the late-morning peak simulated by CAM_ZM (Fig. 1f). While CAM_TDK reasonably captures the nocturnal peak, it also produces an additional noontime maximum. Similar to ZM and TDK, the UNICON scheme also produces a noontime peak in convective precipitation (Fig. 1i), with nocturnal rainfall being primarily contributed by large-scale precipitation.

To understand why SCM simulations produce noontime peaks in convective precipitation, we show in Fig. 2 the cloud-base cumulus mass flux M_b and closure-related quantities in each convection scheme. Note that convective precipitation is proportional to the product of M_b and the updraft rain/snow content, with M_b itself determined by the standard quasi-equilibrium closure as $\frac{\mathrm{CAPE}}{\tau * F}$, where τ is the convective adjustment time scale and F is the CAPE consumption rate per unit mass flux. As noticed, M_b is generally in phase with PCAPE (density-weighted CAPE) in TDK, but shows little phase coherence with CAPE in ZM, both being computed within their respective convection schemes during active convection. Over TP, the ZM M_b peaks near 11:00 LST, well ahead of the CAPE maximum at 18:00 LST, due to the lower F at that time (Fig. S1 in the Supplement). The phase advance of M_b relative to CAPE is even more pronounced over SECN (Fig. 2b). Higher CAPE is usually associated with deeper convection and greater vertically accumulated condensate, which, together with the M_b peak, tends to produce dual precipitation peaks in ZM (Fig. 1h). The UNICON scheme does not rely on any equilibrium assumptions; instead, it initializes the thermodynamic properties of updraft plumes using the input surface flux. In all three regions, the UNICON M_b peaks around 14:00 LST, closely tracking the evolution of the launching vertical velocity derived from the surface turbulent kinetic energy (TKE).

3.2 Modification of Convection Schemes and Their Impact on Diurnal Precipitation

The cloud-base mass flux in ZM and TDK is based on the standard equilibrium closure, which assumes that CAPE

Table 1. Parameterization configurations.

Parameterization		CAM_ZM	CAM_TDK	CAM_UNICON
Deep convection	CTRL	CAPE-based trigger and closure (*Zhang and McFarlane, 1995*)	Equilibrium closure (*Bechtold et al., 2014*)	Cold-pool feedback disabled (*Park, 2014a*)
	SENS	dCAPE trigger + elevated convection (*Xie and Zhang, 2000; Xie et al., 2019*)	Non-equilibrium closure (*Bechtold et al., 2014*)	Cold pool + elevated convection (*Park et al., 2024*)
Shallow convection		*Bretherton and Park (2008)*		*Park (2014a)*
PBL turbulence		*Bretherton and Park (2009)*		
Cloud macrophysics		*Park et al. (2014)*		
Cloud microphysics		*Morrison and Gettelman (2008)*		
Radiation		*Clough et al. (2005)*		

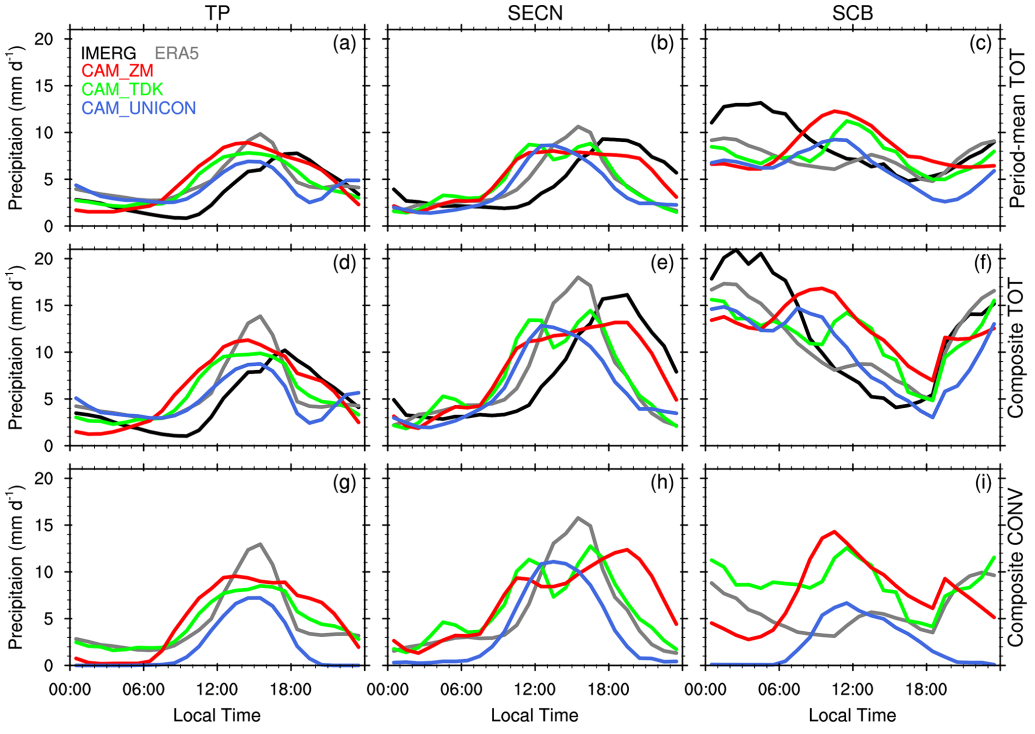


Figure 1. Period-averaged **(a–c)** and case-composite **(d–i)** diurnal precipitation cycles over TP (left), SECN (middle) and SCB (right) from IMERG, ERA5 and the SCM control simulation. Panels **(g–i)** show convective precipitation. In each panel, the red, green, and blue lines represent precipitation simulated by CAM_ZM, CAM_TDK, and CAM_UNICON, respectively.

is consumed at an exponential rate by cumulus convection with characteristic time scale. Donner and Phillips (2003) and Zhang (2002) pointed out that, although a CAPE quasi-equilibrium closure is well-suited for the free troposphere, it does not apply well to the entire troposphere including the boundary layer, particularly under rapidly varying boundary-layer forcing. Indeed, under weak large-scale forcing, boundary layer generation of CAPE dominates surface-driven convection (Bechtold et al., 2014). Hence, the strategy for improvement centers on how to properly account for the imbalance between deep convection and PBL production. Xie and Zhang (2000) addressed this by reducing M_b when dCAPE is below a threshold value of $100\,\mathrm{J\,kg^{-1}\,h^{-1}}$, with the reduction factor linearly related to dCAPE:

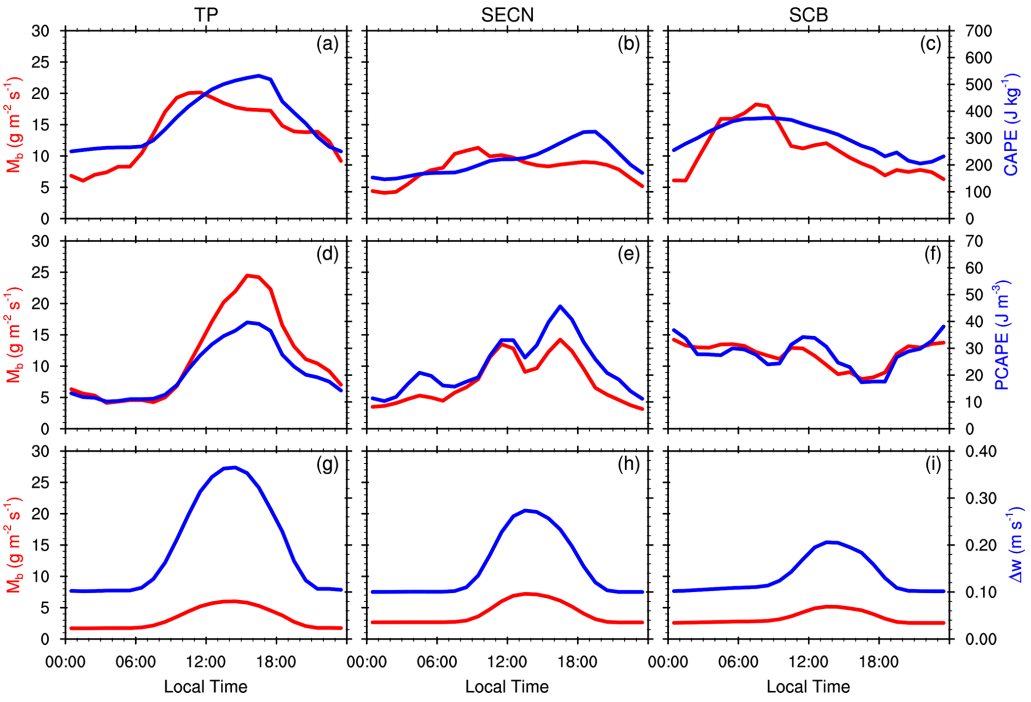


Figure 2. Cloud-base cumulus mass flux M_b and closure-related quantities in the control experiment of **(a–c)** CAM_ZM, **(d–f)** CAM_TDK and **(g–i)** CAM_UNICON over TP (left), SECN (middle) and SCB (right). The closure-related quantities are CAPE for ZM, PCAPE for TDK, and perturbations of updraft vertical velocity driven by symmetric turbulent eddies in the UNICON scheme.

$$M_b = \begin{cases} \dfrac{\text{CAPE}}{\tau \times F} & \text{if dCAPE} > 100 \\ \dfrac{\text{CAPE}}{\tau \times F} \times \dfrac{\text{dCAPE}}{100} & \text{if dCAPE} \leq 100 \end{cases} \quad (1)$$

The underlying reasoning is that when large-scale dynamic forcing is weak, i.e., small positive dCAPE, the convective adjustment time scale is typically larger. Bechtold et al. (2014) addressed this by subtracting from the total mass flux a fraction of shallow convective contribution that is supposed to approximately balance the boundary layer forcing. Park (2014a) attributed the inability to accurately simulate the DCP, in part, to the absence of plume memory under the diagnostic quasi-equilibrium approximation. He then developed an approach that incorporates additional plume memory through the prognostic cold pool and employs this memory to reconstruct convective plumes at subsequent time steps. Figure 3 presents M_b for each scheme in the sensitivity experiment, with the aforementioned modifications applied. A notable change is that for both TP and SECN, the M_b peak shifts to approximately 18:00 LST across all schemes, matching the observed precipitation peak much more closely. Each scheme accomplishes this improvement through a different mechanism. In CAM_ZM, this improvement primarily stems from dCAPE trigger, as for daytime convection, the launching level remains near the surface even though the implementation of elevated convection allows parcels to be launched above PBL. As noticed, dCAPE (dashed lines in Fig. 3a and b) peaks around 18:00 LST and is much smaller near noon, which suppresses the early M_b peak in CTRL and shifts the main maximum toward 18:00 LST. In CAM_TDK, the PBL contribution to PCAPE peaks around 16:00 LST (dashed lines in Fig. 3d and e), accounting for a large portion of the total PCAPE at that time. After subtracting this contribution, the resulting PCAPE and M_b peaks are delayed to 17:00 LST over TP and 19:00 LST over SECN, approximately 1–2 h later than in CTRL. It is worth noting that the dual M_b peak in the control experiment of both CAM_ZM and CAM_TDK over SECN now merges into a single peak. In CAM_UNICON, while the updraft perturbations from symmetric turbulent eddies still peak around noon, the enabled cold-pool-driven mesoscale flow generates pronounced dynamic uplift forcing around 18:00 LST, ultimately shifting the M_b peak toward 18:00 LST.

For elevated convection over SCB, Fig. 4 compares the time-pressure cross-sections of the launching level frequency and updraft mass flux between the control and sensitivity runs. In all control simulations except CAM_TDK, afternoon convection prevails, whereas nocturnal convection remains very weak. Both CAM_ZM and CAM_UNICON restrict the launch level to near the surface, inhibiting convection initialization during nighttime because of the strong nocturnal inversion that develops above the PBL. CAM_TDK, however, is not subject to this restriction. It produces significant

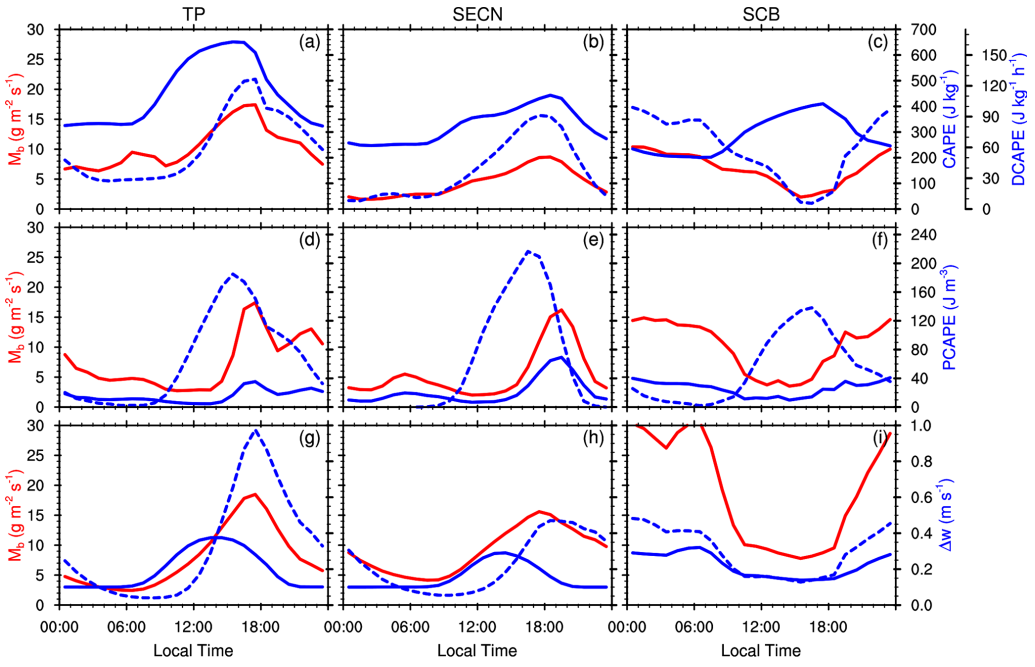


Figure 3. Same as Fig. 2, but for the sensitivity experiments. The dashed blue lines in each row denote, respectively: dCAPE in ZM, the PBL contribution to PCAPE in TDK, and perturbations induced by subgrid cold pools and external mesoscale upflow in UNICON.

updraft mass during nighttime and early morning, frequently triggering elevated convection below 800 hPa (Fig. 4b). Notably, sporadic launching-level peaks occur at levels ever higher than 600 hPa, directly related to the TDK's treatment of mid-level convection. Removing the boundary-layer origin constraint in ZM and UNICON leads to stronger nocturnal convection, weaker afternoon convection, and a markedly raised launch level relative to the control runs (Fig. 4d and f). This improvement is also manifested in the diurnal variation of M_b (rightmost column of Fig. 3), with a maximum at night and a minimum around midday. Most strikingly, CAM_TDK also yields stronger nocturnal convection in the sensitivity run (Fig. 4e), likely because the exclusion of PBL-contributed PCAPE (Fig. 3f) suppresses daytime convection, thereby favoring subsequent nocturnal development.

Figure 5 compares the DCP simulation between CTRL and SENS experiments. As anticipated, all modifications result in improved diurnal precipitation cycles when compared with the control runs. For all three schemes, the premature afternoon precipitation over TP and SECN is substantially delayed, aligning better with observations. This delayed response is largely attributable to the delay in simulated convective precipitation (dashed lines). Note the stronger precipitation in the CAM_UNICON sensitivity experiment is due to positive perturbations in updraft vertical velocity, temperature, and moisture, driven by mesoscale organized flow (Park, 2014b; Wang et al., 2026). Over SCB, the excessive afternoon rainfall and insufficient nocturnal precipitation in the control experiments of CAM_ZM and CAM_UNICON are substantially improved in the sensitivity experiments. Although no explicit modification is made for elevated convection in CAM_TDK, nocturnal precipitation is also enhanced in the sensitivity experiment (Fig. 5f), presumably due to the reduced afternoon convective stabilization resulting from the removal of shallow convective contribution in the closure. A similar daytime-to-nocturnal convective interaction has also been documented by Xie et al. (2019) and Park et al. (2024), who found that suppressing daytime convection can strengthen nocturnal precipitation.

We note that each sensitivity experiment for ZM and UNICON modifies two factors simultaneously. For example, in CAM_ZM, the M_b scaling that primarily tagets afternoon convection also influences nocturnal convection. To address this confounding issue, we performed additional isolated experiments and examined the individual contributions. The trigger-only experiment behaves similarly to CTRL and does not improve nocturnal precipitation (purple curves in Fig. S2a and b in the Supplement). In contrast, the elevated-convection-only experiment captures the nocturnal precipitation peak but overestimates daytime precipitation. Only the combined experiment, which includes both the dCAPE trigger and elevated convection, reproduces the nocturnal precipitation peak as well as the daytime precipitation minimum well. For UNICON, we conducted a similar set of experiments but did not isolate the elevated-convection-only case, because elevated convection is intrinsically coupled to the cold-pool-driven mesoscale flow in this scheme. The cold-pool feedback alone substantially enhances convective pre-

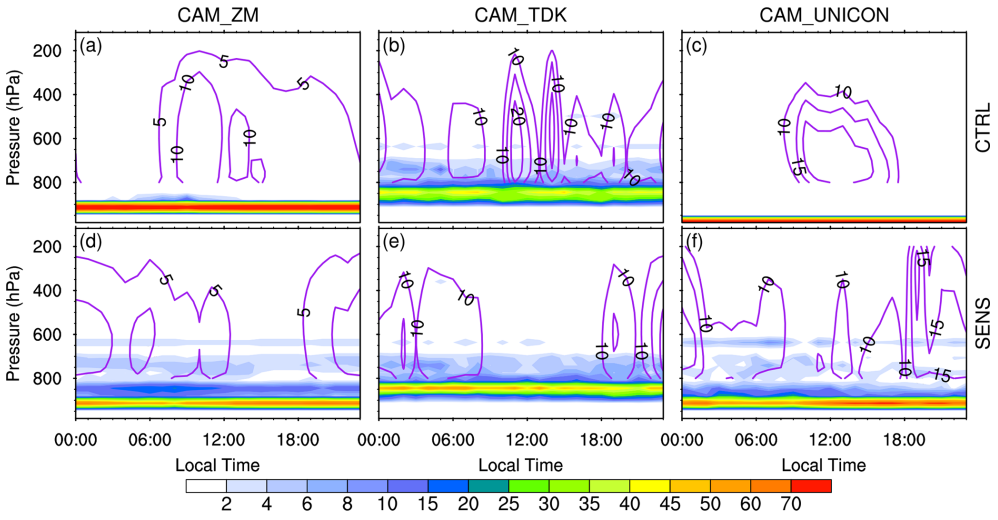


Figure 4. Time-pressure cross-sections of launching-level frequency (shaded, units: %) and updraft mass flux (contour, units: $g\,m^{-2}\,s^{-1}$) over SCB for the control (top) and sensitivity (bottom) experiments. From left to right, the panels show results from CAM_ZM, CAM_TDK, and CAM_UNICON, respectively.

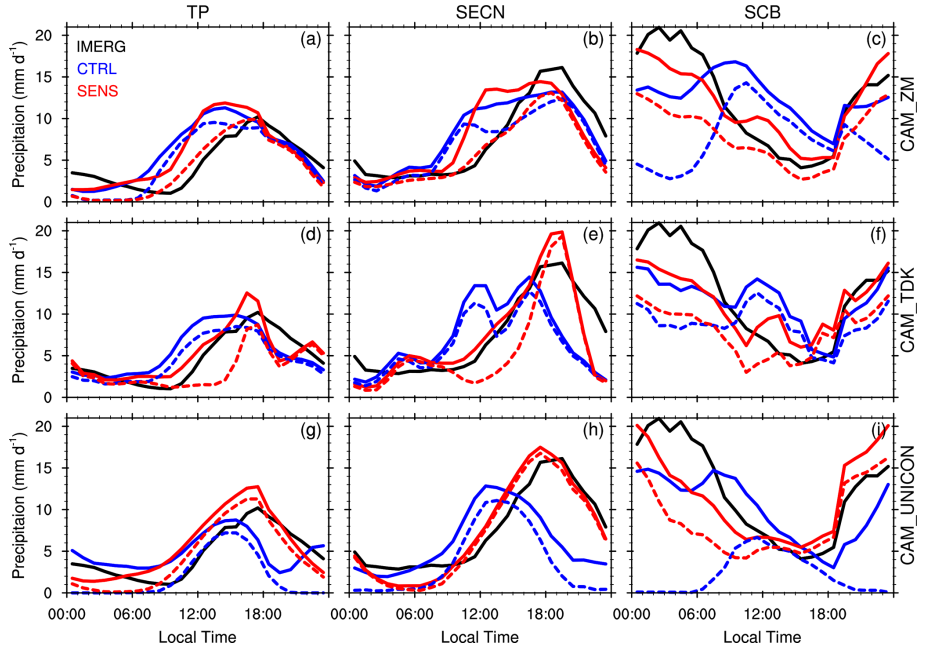


Figure 5. Diurnal cycles of total (solid) and convective (dashed) precipitation over TP (left), SECN (middle), and SCB for the control (blue) and sensitivity (red) runs of each convection scheme. From top to bottom, the panels show DCP simulated by CAM_ZM, CAM_TDK, and CAM_UNICON, respectively.

cipitation relative to CTRL (Fig. S2d). However, total nocturnal precipitation is slightly lower than in CTRL (Fig. S2c). Therefore, the improvement in nocturnal precipitation is achieved only when elevated convection is included.

4 Diurnal Variation of Diabatic Heating

To examine the impact of modified convection schemes on diabatic heating, Fig. 6 presents the diurnal cycles of apparent heating Q_1 and moisture sink Q_2 over TP for both control and sensitivity experiments. These quantities are computed as the sum of tendencies from individual parameterizations. A common feature is the upward-tilting Q_1 structure,

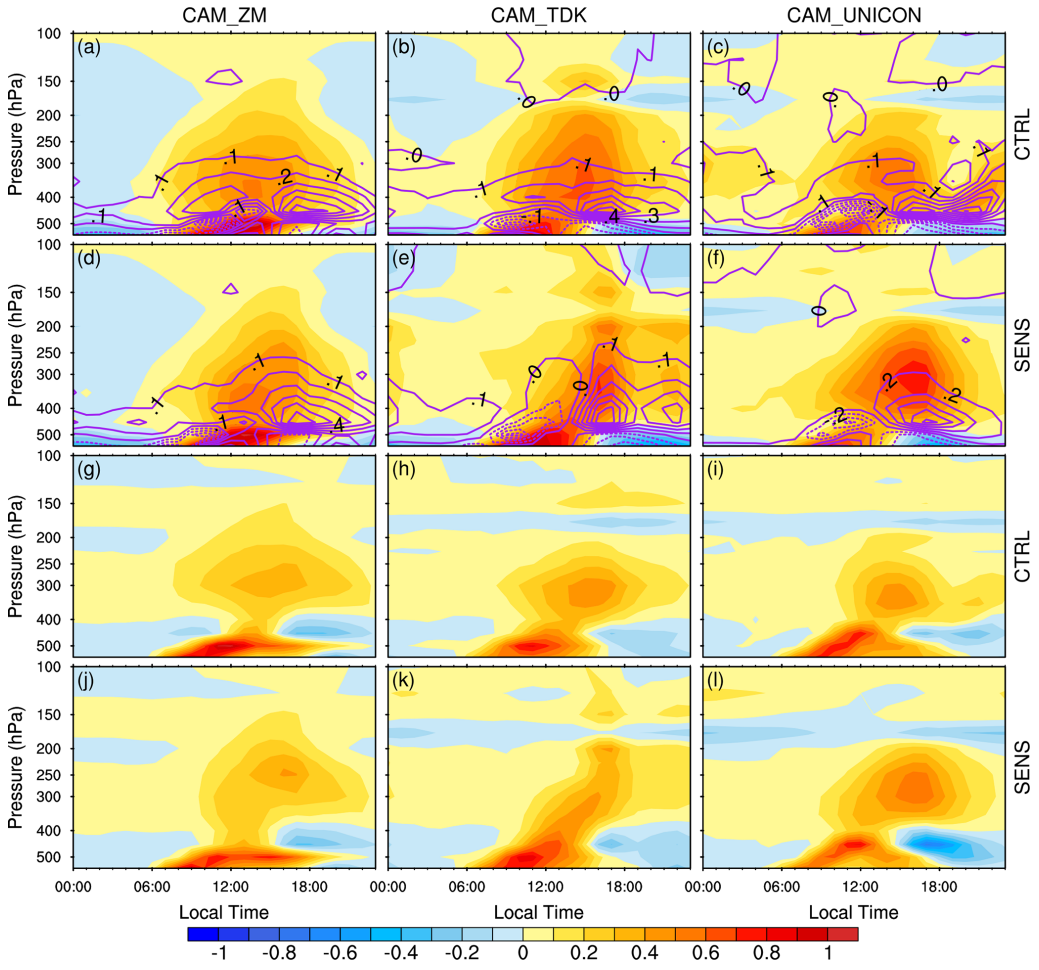


Figure 6. The diurnal cycles of **(a–f)** apparent heating Q_1 (shaded), moisture sink Q_2 (contour) and **(g–l)** subgrid-scale MSE transport $Q_1 - Q_2 - Q_{\mathrm{rad}}$ over TP for both control and sensitivity experiments. From left to right, the panels show results from CAM_ZM, CAM_TDK, and CAM_UNICON, respectively. In the upper two panels, solid lines are for contours greater than or equal to zero and dashed lines for contours less than zero. Units: $\mathrm{K\,h^{-1}}$.

which extends from PBL in the morning to mid-tropospheric levels later in the day. This evolution features an early stage with positive Q_1 and negative Q_2 in the lower troposphere, followed by a transition to positive values for both Q_1 and Q_2 aloft once deep convection develops. Although all SCMs reasonably reproduce this upward-tilting structure, they differ notably in the timing and height of the peak heating. Relative to their control experiments, CAM_TDK and CAM_UNICON delay and elevate the heating peak, resulting in a more pronounced upward-tilt structure (Fig. 6e and f). Moreover, CAM_UNICON exhibits a stronger heating amplitude, consistent with its intensified convection. While the ZM heating center shows no clear phase shift between the control and sensitivity experiments, it tends to extend upward to higher altitudes over time in the sensitivity run (Fig. 6d). Notably, the noontime Q_2 peak near 400 hPa is strongly suppressed in all sensitivity experiments, thereby alleviating the overly strong early-afternoon precipitation in the control. The lower positioning of the Q_2 peak relative to Q_1 is indicative of pronounced subgrid-scale MSE transport, which is presented in the bottom two rows of Fig. 6 as the term $Q_1 - Q_2 - Q_{\mathrm{rad}}$, where Q_{rad} denotes radiative heating. After sunrise, $Q_1 - Q_2 - Q_{\mathrm{rad}}$ is initially positive and continues to rise due to subgrid-scale transport from turbulence and shallow convection. As the cycle progresses, a characteristic dipole structure emerges in its vertical profile – negative anomalies dominate below 400 hPa, while positive anomalies prevail aloft – a typical signature of well-organized deep convection. All three schemes show a more pronounced upward-tilting structure in the sensitivity experiment than in the control, owing to the delayed onset of deep convection.

Similar discrepancies between control and sensitivity runs are also evident over SECN (Fig. 7). All sensitivity runs exhibit a suppression of the early Q_2 peak, accompanied by a delayed and elevated Q_1 peak and a more pronounced upward-tilting structure in subgrid-scale MSE transport. It

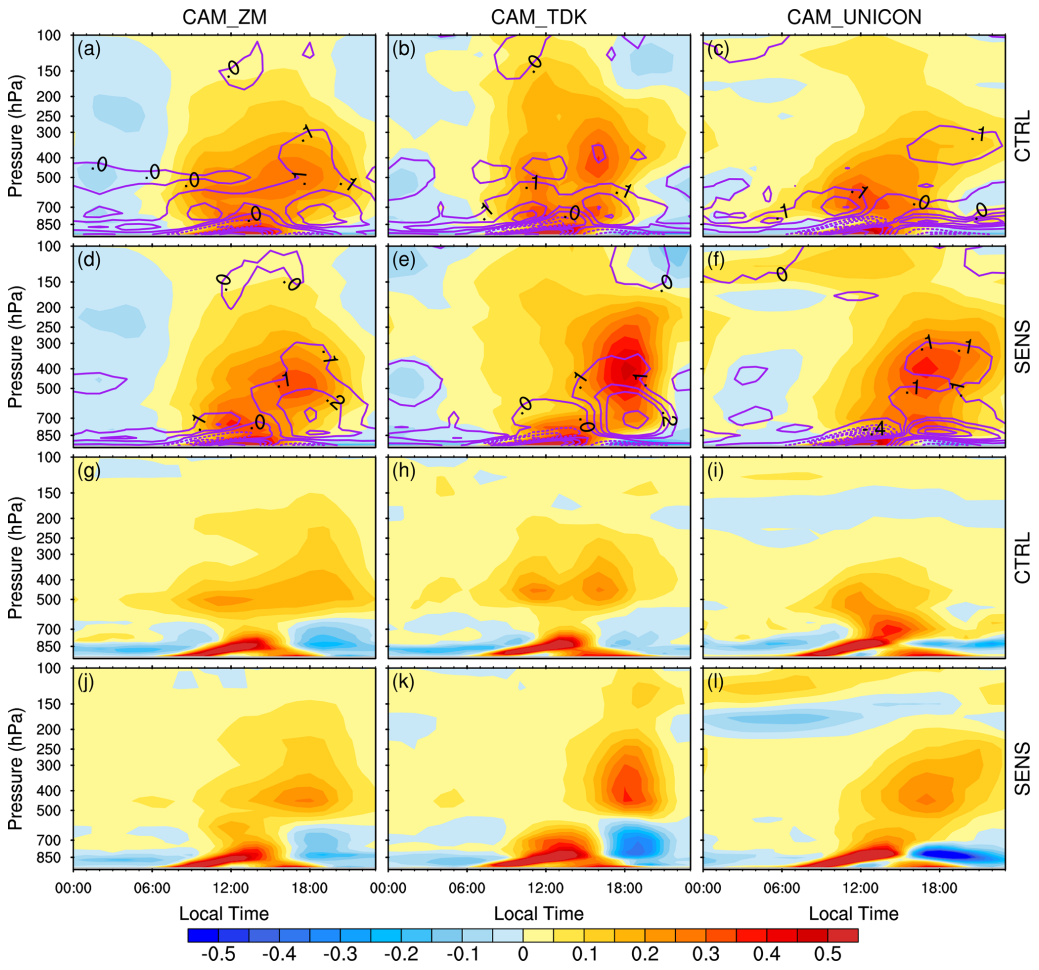


Figure 7. Same as Fig. 6, but for SECN.

is worth noting that CAM_UNICON exhibits more coherent vertical organization in subgrid-scale MSE transport than CAM_ZM and CAM_TDK, particularly during the transition from shallow to deep convection, underscoring the benefit of UNICON's unified convection framework. Figure 8 presents the diurnal cycles of diabatic heating over SCB, where a notable difference from TP and SECN is the dominance of nocturnal heating. This nocturnal heating in the control runs of CAM_ZM and CAM_UNICON is primarily due to large-scale condensation, as indicated by the relatively weak subgrid-scale MSE transport at night (Fig. 8g and i). In contrast, the stronger MSE transport in CAM_TDK (Fig. 8h) suggests that convection contributes substantially to its heating. All sensitivity experiments exhibit enhanced nocturnal convection, with both Q_1 and subgrid-scale MSE transport strengthened during nighttime. Conversely, the diabatic heating at noontime is substantially suppressed, in line with the reduced precipitation at that time.

5 Impact of Convection Scheme Modifications on Thermodynamic Fields

While the modified convection schemes improve the diurnal phase of precipitation and associated diabatic heating, they also tend to produce deep and/or stronger convection, particularly in CAM_UNICON. To assess whether these changes have an adverse impact on temperature and moisture biases, we examine the model's thermodynamic performance in this section.

5.1 Diurnally Averaged Q_1 and Q_2: Simulation vs. ERA5

Figure 9 compares the simulated diurnally averaged Q_1 and Q_2 profiles against ERA5-derived ones, along with their deep convective contributions in each SCM. The Q_1 and Q_2 derived from ERA5 reanalysis are calculated as residuals of the thermodynamic equation and moisture continuity equation, following Yanai et al. (1973). Relative to ERA5, the CAM_TDK control run over TP exhibits a positive Q_1 bias of approximately $2\,\mathrm{K\,d^{-1}}$ throughout the troposphere

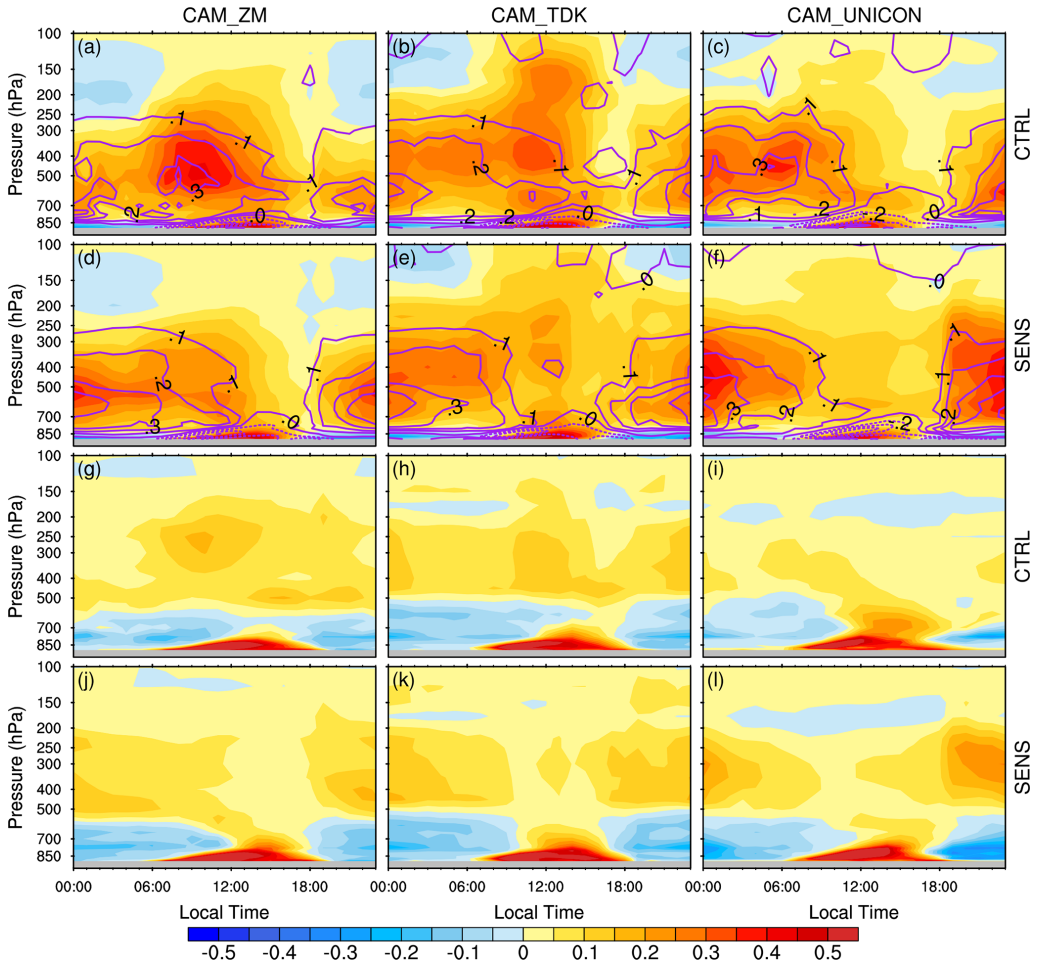


Figure 8. Same as Fig. 6, but for SCB.

and a negative Q_2 bias of approximately $2\,\mathrm{K\,d^{-1}}$ between 400 and 450 hPa (Fig. 9d). While these biases are considerably alleviated in the sensitivity experiment below 450 hPa, a positive Q_1 bias is exaggerated aloft, largely a consequence of convection penetrating to higher altitudes. The CAM_UNICON control run exhibits a bias pattern similar to that of CAM_TDK (Fig. 9g), yet the biases are further amplified in the sensitivity run, as a result of the strengthened deep-convective component. The ZM scheme shows a notably smaller Q_1 bias than TDK and UNICON above 450 hPa, yet exhibits a pronounced positive bias of up to $6\,\mathrm{K\,d^{-1}}$ near 500 hPa (Fig. 9a). While the Q_1 and Q_2 profiles remain broadly comparable between the control and sensitivity experiments, the convective component is notably weaker in the latter, implying that other physical processes (e.g., large-scale condensation) compensate for the reduced convective heating (Wang and Zhang, 2013). Over SECN, the Q_1 simulations from all SCMs show better overall performance than over TP, with biases remaining mostly within $\pm 1\,\mathrm{K\,d^{-1}}$. Compared with ERA5, all simulations systematically overestimate Q_2 in the lower troposphere and underestimate it in the upper troposphere. As over the TP, the convective component in the sensitivity runs of CAM_TDK and CAM_ZM extends to higher altitudes, while in CAM_UNICON it is both intensified and extends further upward. For nocturnal convection over SCB, the ZM scheme performs satisfactorily for Q_2, yet exhibits a positive Q_1 bias below 500 hPa and a negative bias above. In contrast, CAM_UNICON simulates Q_1 well, but substantially underestimates Q_2 across the entire troposphere. In comparison, CAM_TDK exhibits overall good agreement with ERA5 for both Q_1 and Q_2. While the modifications substantially improve Q_2 in UNICON, they yield no marked improvement in Q_1 for ZM. It should be noted that the ERA5 reference used here carries inherent uncertainties associated with its convection scheme. By definition, Q_1 and Q_2 are derived as residuals of the thermodynamic and moisture continuity equations, both of which involve vertical advection terms. Vertical advection depends on vertical velocity, which is itself strongly influenced by the model's physical parameterizations – especially convection. For example, if convection is under-represented in ERA5, the

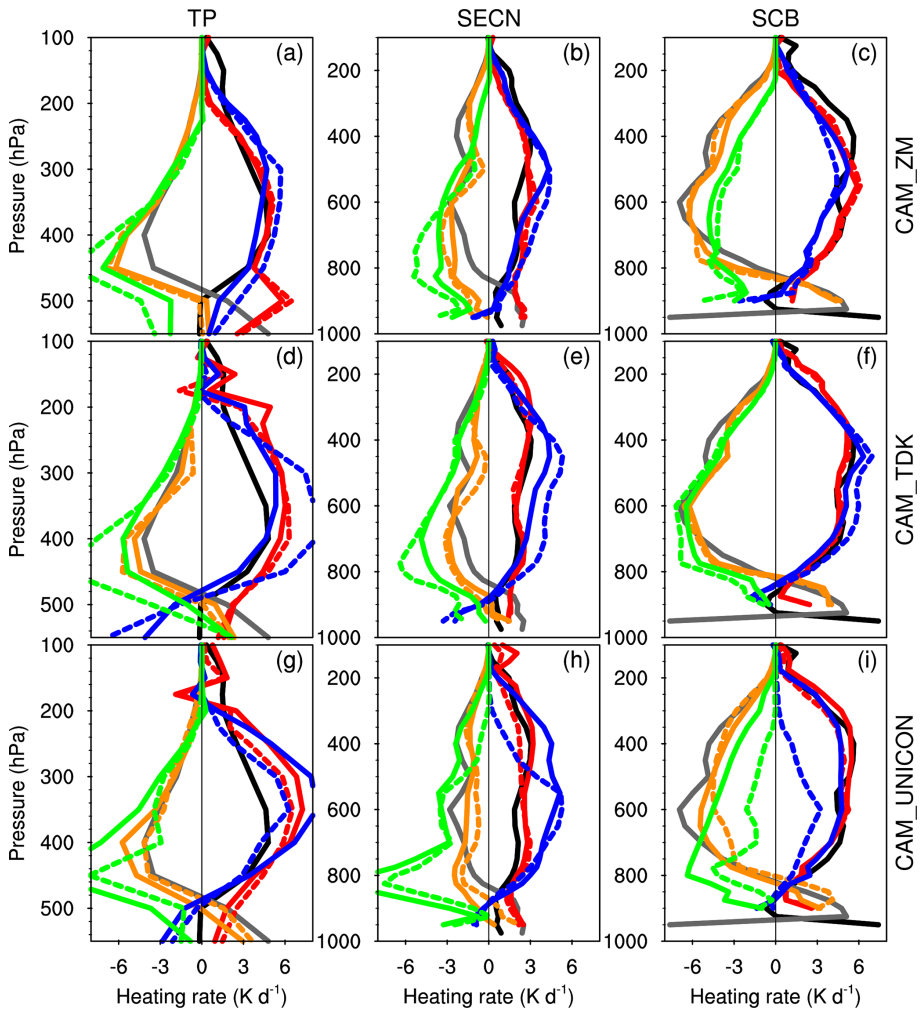


Figure 9. Simulated profiles of Q_1 (red) and Q_2 (orange) compared with ERA5 (black for Q_1, gray for Q_2), along with the deep convective component of Q_1 (blue) and Q_2 (green) in each SCM. Dashed and solid lines denote the control and sensitivity experiments, respectively. From top to bottom, the panels show results from CAM_ZM, CAM_TDK, and CAM_UNICON, respectively. Units: $\mathrm{K\,d^{-1}}$.

associated vertical velocity would be weaker, leading to an underestimation of Q_1 and Q_2.

5.2 Temperature and Moisture Biases

Figures 10 and 11 show the temperature and moisture differences, respectively, between the control run and ERA5 reanalysis (shaded), overlaid with the sensitivity-control differences (contours). Over TP, all three schemes exhibit a band of cold bias of up to 2 K in the upper troposphere during the late afternoon, as well as cold biases of similar magnitude near the surface at noon. Note that the surface cold bias is accompanied by a dry bias of $-1\,\mathrm{g\,kg^{-1}}$, reflecting excessive subgrid-scale MSE transport at noon. A dry bias is also found around 400 hPa after 18:00 LST in CAM_ZM and CAM_TDK, which is consistent with their excessive precipitation relative to ERA5 (Fig. 1d). In the sensitivity experiments, the upper-level cold bias in CAM_TDK and CAM_UNICON is substantially reduced (Fig. 10d and g), consistent with the enhanced Q_1 above 250 hPa (Fig. 9d and g). The ZM scheme exhibits no significant differences, owing to the close resemblance in Q_1 between the two runs (Fig. 9a). The late-afternoon dry bias is also alleviated in the modified TDK and ZM schemes (Fig. 11a and d). In CAM_UNICON, the delayed onset and enhanced intensity of convection in the sensitivity run cause the original mid-to-lower tropospheric wet bias into a dry bias (Figs. 11g and S3g in the Supplement). The bias patterns over SECN are broadly analogous to those over TP, characterized by a cold bias above 200 hPa, a cold and dry bias near the surface at noontime, and a negative moisture bias in the lower troposphere during the late afternoon. Moreover, a warming bias between 200 and 700 hPa around noon is present in all three schemes, which is linked to excessive early-afternoon convection. This bias is largely alleviated in the modified runs, as reflected by the negative SENS-CTRL differences (dashed

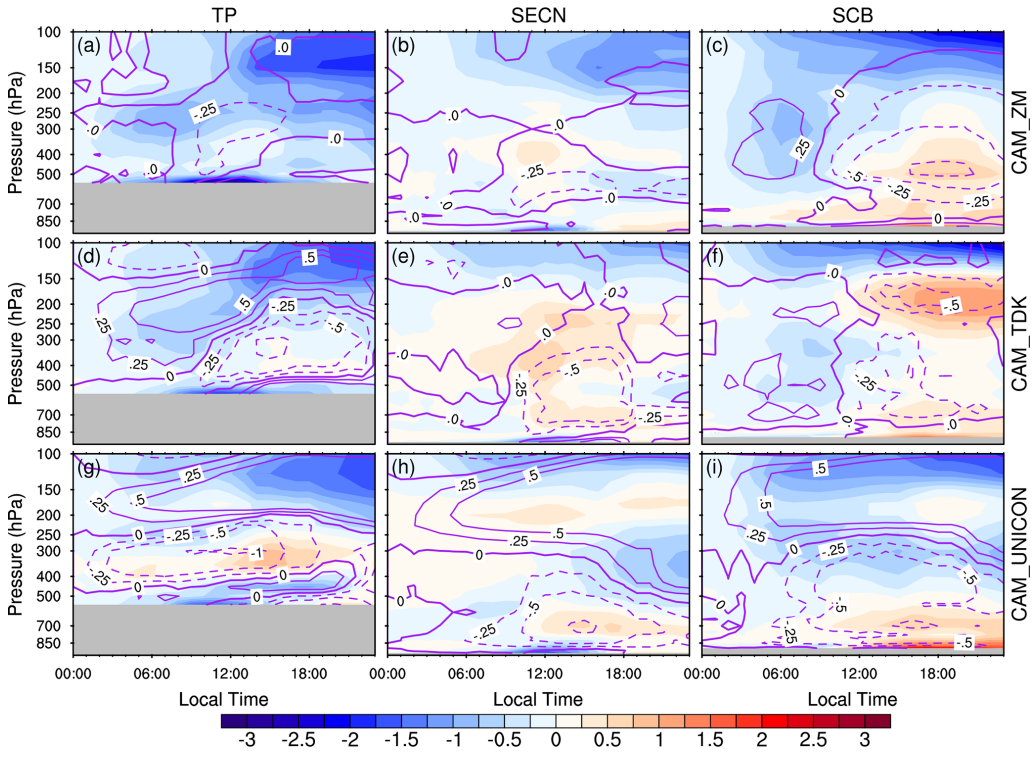


Figure 10. Temperature differences between the control run and ERA5 reanalysis (CTRL–ERA5, shading) and between the sensitivity and control runs (SENS–CTRL, contours) over TP (left), SECN (middle), and SCB (right). Panels from top to bottom show results from CAM_ZM, CAM_TDK, and CAM_UNICON. In these figures, solid lines are for contours greater than or equal to zero and dashed lines for contours less than zero. Units: K.

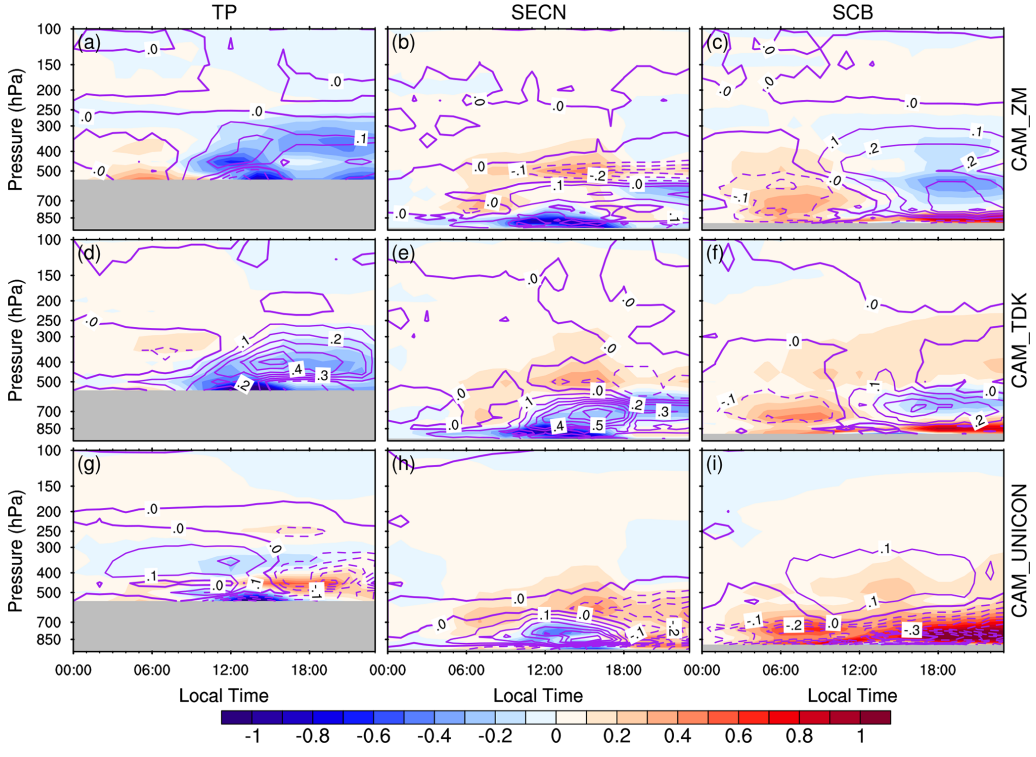


Figure 11. Same as Fig. 10, but for specific humidity (units: $g\,kg^{-1}$).

lines in the middle column of Fig. 10), owing to the suppression of early convective activity. As over the TP, the lower-tropospheric dry bias after 18:00 LST is also reduced in the modified TDK and ZM schemes (Fig. 11b and e). In CAM_UNICON, the temperature differences between sensitivity and control runs are generally opposite in sign to the control bias, largely offsetting the bias (Fig. 10h). Nevertheless, the magnitude of these differences is so large that the sign is reversed completely, leaving a residual warm bias aloft and a cold bias in the lower troposphere (Fig. S4h in the Supplement). Over SCB, the mid-tropospheric warm and dry bias in CAM_ZM is substantially alleviated in the sensitivity run (Figs. 10c and 11c), owing to the suppression of overly active early-afternoon convection. Isolated experiments indicate that the dCAPE trigger helps mitigate the late-afternoon warm and dry biases in CTRL, with active nocturnal convection over SCB further reducing them (Figs. S5a and S6 in the Supplement). In the UNICON sensitivity run, the overly strengthened convection warms the upper troposphere, yielding a positive bias of up to 2.5 K (Fig. S3i), similar to that over TP and SECN. The Q_1 profiles (Fig. S5b), together with the temperature biases in Fig. S7 in the Supplement indicate that the warm bias seen in the UNICON sensitivity run is attributable to cold-pool feedback. This raises a caveat for the UNICON scheme: while enabling cold-pool feedback may improve the diurnal cycle, the overly strong intensity, stemming from positive perturbations in plume initialization, may adversely affect thermodynamic fields.

6 Conclusions

Using a single-column model, this study investigates the impact of convective trigger and closure treatments on the summertime diurnal cycle of precipitation over China, with a focus on three convection schemes: ZM, TDK, and UNICON. The analysis targets two regions characterized by late-afternoon rainfall (TP and SECN) and one region with a nocturnal regime (SCB). Over TP and SECN, the TDK and ZM schemes with the standard CAPE closure simulate precipitation peaks that are substantially earlier than the observed. The UNICON scheme, with cold-pool feedback deactivated, also exhibits a noontime peak, albeit with a somewhat delayed initiation relative to ZM and TDK. Over SCB, both ZM and UNICON produce a pronounced noontime precipitation peak, in stark contrast to the observed nocturnal maximum. TDK reasonably reproduces the nocturnal peak, yet it also produces an additional noontime maximum. These SCM precipitation behaviors are closely related to closure assumptions and the resulting cloud-base mass flux. While convective precipitation in ZM and TDK is more closely tied to CAPE, in UNICON it aligns more directly with the surface fluxes.

Modifications were then applied to each scheme: adopting the dCAPE trigger and permitting elevated convection in ZM; activating cold-pool feedback and allowing elevated convection in UNICON; and applying the non-equilibrium closure in TDK. A notable improvement is evident for both late-afternoon and nocturnal rainfall. Over TP and SECN, the precipitation peak shifts to approximately 18:00 LST across all schemes, aligning much more closely with the observation. Each scheme achieves this improvement through a distinct mechanism. In ZM, the dCAPE constraint suppresses the early peak at 10:00 LST and redirects the main peak toward 18:00 LST. In TDK, subtracting the boundary-layer contribution to PCAPE delays the precipitation peak to 19:00 LST. In UNICON, the cold-pool-driven mesoscale flow generates pronounced dynamic uplift forcing around 18:00 LST, ultimately shifting the peak toward that time. Over SCB, permitting convection to be launched above PBL in ZM and UNICON enhances nocturnal convection while suppressing afternoon convection. Although no explicit modification is made for elevated convection in TDK, applying the non-equilibrium closure also enhances nocturnal precipitation, due to the reduced convective stabilization in the afternoon.

The improved diurnal cycle is manifested in the diabatic heating fields as well. All modifications lead to a delayed and more pronounced upward-tilting Q_1 heating structure. Subgrid-scale MSE transport is likewise delayed and more upward tilted, with ZM and TDK extending to higher altitudes, while in UNICON it is both intensified and extends further upward. These changes alleviate the upper-level cold bias in TDK and ZM and largely reduce the late-afternoon dry bias in the lower troposphere. However, the overly strengthened convection in UNICON yields a warm bias of up to 2.5 K in the upper troposphere, as the positive perturbations in plume properties induced by mesoscale organized flow are too strong and deteriorate the thermodynamic fields.

Data availability. The simulation data used in this study are available at https://doi.org/10.5281/zenodo.21207758 (Wang and Liu, 2026).

Supplement. The supplement related to this article is available online at https://doi.org/10.5194/acp-26-14471-2026-supplement.

Author contributions. XW: conceptualization, funding acquisition, methodology, validation, writing (original draft, review and editing). YaL: data curation, visualization, writing (review and editing). YiL: resources, writing (review and editing).

Competing interests. The contact author has declared that none of the authors has any competing interests.

Disclaimer. Publisher's note: Copernicus Publications remains neutral with regard to jurisdictional claims made in the text, published maps, institutional affiliations, or any other geographical representation in this paper. The authors bear the ultimate responsibility for providing appropriate place names. Views expressed in the text are those of the authors and do not necessarily reflect the views of the publisher.

Acknowledgements. The authors would like to thank the two anonymous reviewers for their constructive comments that helped to clarify and improve the original paper. The authors also thank the GPM, ERA5, NCAR science teams for providing the data and model used in this study.

Financial support. This research is jointly supported by the National Key Research and Development Program of China (grant no. 2022YFF0802003), the National Natural Science Foundation of China (grant no. 42575163), and the National Key Scientific and Technological Infrastructure project "Earth System Science Numerical Simulator Facility" (EarthLab).

Review statement. This paper was edited by Shaocheng Xie and reviewed by two anonymous referees.

References

Bechtold, P., Semane, N., Lopez, P., Chaboureau, J.-P., Beljaars, A., and Bormann, N.: Representing Equilibrium and Nonequilibrium Convection in Large-Scale Models, J. Atmos. Sci., 71, 734–753, https://doi.org/10.1175/JAS-D-13-0163.1, 2014.

Benedict, J. J., Maloney, E. D., Sobel, A. H., Frierson, D. M., and Donner, L. J.: Tropical Intraseasonal Variability in Version 3 of the GFDL Atmosphere Model, J. Climate, 26, 426–449, https://doi.org/10.1175/JCLI-D-12-00103.1, 2013.

Bretherton, C. S. and Park, S.: A New Bulk Shallow-Cumulus Model and Implications for Penetrative Entrainment Feedback on Updraft Buoyancy, J. Atmos. Sci., 65, 2174–2193, https://doi.org/10.1175/2007JAS2242.1, 2008.

Bretherton, C. S. and Park, S.: A New Moist Turbulence Parameterization in the Community Atmosphere Model, J. Climate, 22, 3422–3448, https://doi.org/10.1175/2008JCLI2556.1, 2009.

Carbone, R. E. and Tuttle, J. D.: Rainfall Occurrence in the U. S. Warm Season: The Diurnal Cycle, J. Climate, 21, 4132–4146, https://doi.org/10.1175/2008JCLI2275.1, 2008.

Chen, G., Sha, W., Iwasaki, T., and Wen, Z.: Diurnal Cycle of a Heavy Rainfall Corridor over East Asia, Mon. Weather Rev., 145, 3365–3389, https://doi.org/10.1175/MWR-D-16-0423.1, 2017.

Clough, S. A., Shephard, M. W., Mlawer, E. J., Delamere, J. S., Iacono, M. J., Cady-Pereira, K., Boukabara, S., and Brown, P. D.: Atmospheric radiative transfer modeling: A summary of the AER codes, J. Quant. Spectrosc. Ra., 91, 233–244, https://doi.org/10.1016/j.jqsrt.2004.05.058, 2005.

Dai, A. and Trenberth, K. E.: The Diurnal Cycle and Its Depiction in the Community Climate System Model, J. Climate, 17, 930–951, https://doi.org/10.1175/1520-0442(2004)017<0930:TDCAID>2.0.CO;2, 2004.

Dai, A., Giorgi, F., and Trenberth, K. E.: Observed and model-simulated diurnal cycles of precipitation over the contiguous United States, J. Geophys. Res.-Atmos., 104, 6377–6402, https://doi.org/10.1029/98JD02720, 1999.

Dai, A.: Precipitation characteristics in eighteen coupled climate models, J. Climate, 19, 4605–4630, https://doi.org/10.1175/JCLI3884.1, 2006.

Davies, L., Plant, R. S., and Derbyshire, S. H.: Departures from convective equilibrium with a rapidly varying surface forcing, Q. J. Roy. Meteor. Soc., 139, 1731–1746, https://doi.org/10.1002/qj.2065, 2013.

Donner, L. J. and Phillips, V. T.: Boundary layer control on convective available potential energy: Implications for cumulus parameterization, J. Geophys. Res.-Atmos., 108, https://doi.org/10.1029/2003JD003773, 2003.

Gettelman, A., Truesdale, J. E., Bacmeister, J. T., Caldwell, P. M., Neale, R. B., Bogenschutz, P. A., and Simpson, I. R.: The single column atmosphere model version 6 (SCAM6): Not a scam but a tool for model evaluation and development, J. Adv. Model. Earth Sy., 11, 1381–1401, https://doi.org/10.1029/2018MS001578, 2019.

Hersbach, H., Bell, B., Berrisford, P., Hirahara, S., Horányi, A., Muñoz-Sabater, J., Nicolas, J., Peubey, C., Radu, R., Schepers, D., Simmons, A., Soci, C., Abdalla, S., Abellan, X., Balsamo, G., Bechtold, P., Biavati, G., Bidlot, J., Bonavita, M., De Chiara, G., Dahlgren, P., Dee, D., Diamantakis, M., Dragani, R., Flemming, J., Forbes, R., Fuentes, M., Geer, A., Haimberger, L., Healy, S., Hogan, R. J., Hólm, E., Janisková, M., Keeley, S., Laloyaux, P., Lopez, P., Lupu, C., Radnoti, G., De Rosnay, P., Rozum, I., Vamborg, F., Villaume, S., and Thépaut, J.: The ERA5 global reanalysis, Q. J. Roy. Meteor. Soc., 146, 1999–2049, https://doi.org/10.1002/qj.3803, 2020.

Huffman, G. J., Stocker, E. F., Bolvin, D. T., Nelkin, E. J., and Tan, J.: GPM IMERG Final Precipitation L3 Half Hourly $0.1° \times 0.1°$ V07, Greenbelt, MD, Goddard Earth Sciences Data and Information Services Center (GES DISC) [data set], https://doi.org/10.5067/GPM/IMERG/3B-HH/07, 2023.

Lee, M.-I., Schubert, S. D., Suarez, M. J., Held, I. M., Lau, N.-C., Ploshay, J. J., Kumar, A., Kim, H.-K., and Schemm, J.-K. E.: An analysis of the warm-season diurnal cycle over the continental United States and northern Mexico in general circulation models, J. Hydrometeorol., 8, 344–366, https://doi.org/10.1175/JHM581.1, 2007.

Lee, M.-I., Schubert, S. D., Suarez, M. J., Schemm, J.-K. E., Pan, H.-L., Han, J., and Yoo, S.-H.: Role of convection triggers in the simulation of the diurnal cycle of precipitation over the United States Great Plains in a general circulation model, J. Geophys. Res.-Atmos., 113, D02111, https://doi.org/10.1029/2007JD008984, 2008.

Li, J., Yu, R., and Zhou, T.: Seasonal variation of the diurnal cycle of rainfall in southern contiguous China, J. Climate, 21, https://doi.org/10.1175/2008JCLI2188.1, 2008.

Liu, Y., Wang, X., Liu, Y., Tang, S., and Miao, H.: A process-oriented analysis of the summertime diurnal cycle of precipitation and diabatic heating over China in three reanalyses, Atmos. Chem. Phys., 26, 6763–6779, https://doi.org/10.5194/acp-26-6763-2026, 2026.

Mapes, B., Tulich, S., Lin, J., and Zuidema, P.: The mesoscale convection life cycle: Building block or prototype for large-scale tropical waves?, Dynam. Atmos. Oceans, 42, 3–29, https://doi.org/10.1016/j.dynatmoce.2006.03.003, 2006.

Morrison, H. and Gettelman, A.: A New Two-Moment Bulk Stratiform Cloud Microphysics Scheme in the Community Atmosphere Model, Version 3 (CAM3). Part I: Description and Numerical Tests, J. Climate, 21, 3642–3659, https://doi.org/10.1175/2008JCLI2105.1, 2008.

Park, S.: A Unified Convection Scheme (UNICON). Part I: Formulationm, J. Atmos. Sci., 71, 3902–3930, https://doi.org/10.1175/JAS-D-13-0233.1, 2014a.

Park, S.: A unified convection scheme (UNICON). Part II: Simulation, J. Atmos. Sci., 71, 3931–3973, https://doi.org/10.1175/JAS-D-13-0234.1, 2014b.

Park, S. and Bretherton, C. S.: The University of Washington Shallow Convection and Moist Turbulence Schemes and Their Impact on Climate Simulations with the Community Atmosphere Model, J. Climate, 22, 3449–3469, https://doi.org/10.1175/2008JCLI2557.1, 2009.

Park, S., Bretherton, C. S., and Rasch, P. J.: Integrating Cloud Processes in the Community Atmosphere Model, Version 5, J. Climate, 27, 6821–6856, https://doi.org/10.1175/JCLI-D-14-00087.1, 2014.

Park, S., Song, C., Kim, S., and Kim, J.: Parameterization of the elevated convection with a unified convection scheme (UNICON) and its impacts on the diurnal cycle of precipitation, J. Adv. Model. Earth Sy., 16, e2023MS003651, https://doi.org/10.1029/2023MS003651, 2024.

Tang, S., Xie, S., Guo, Z., Hong, S., Khouider, B., Klocke, D., Köhler, M., Koo, M., Krishna, P. M., Larson, V. E., Park, S., Vaillancourt, P. A., Wang, Y., Yang, J., Daleu, C. L., Homeyer, C. R., Jones, T. R., Malap, N., Neggers, R., Prabhakaran, T., Ramirez, E., Schumacher, C., Tao, C., Bechtold, P., Ma, H., Neelin, J. D., and Zeng, X.: Long-term single-column model intercomparison of diurnal cycle of precipitation over midlatitude and tropical land, Q. J. Roy. Meteor. Soc., 148, 641–669, https://doi.org/10.1002/qj.4222, 2022.

Tiedtke, M.: A comprehensive mass flux scheme for cumulus parameterization in large-scale models, Mon. Weather Rev., 117, 1779–1800, https://doi.org/10.1175/1520-0493(1989)117<1779:ACMFSF>2.0.CO;2, 1989.

Trenberth, K. E., Dai, A., Rasmussen, R. M., and Parsons, D. B.: The changing character of precipitation, B. Am. Meteorol. Soc., 84, 1205–1218, https://doi.org/10.1175/BAMS-84-9-1205, 2003.

van Stratum, B. J. H., van Heerwaarden, C. C., and Vilà-Guerau de Arellano, J.: The Benefits and Challenges of Downscaling a Global Reanalysis with Doubly-Periodic Large-Eddy Simulations, J. Adv. Model. Earth Sy., 15, e2023MS003750, https://doi.org/10.1029/2023MS003750, 2023.

Wang, X. and Liu, Y.: Simulation Data for the Sensitivity of Summertime Diurnal Precipitation Cycle over China to Convective Trigger and Closure Treatments in a Single-Column Model, Zenodo [data set], https://doi.org/10.5281/zenodo.21207758, 2026.

Wang, X. and Zhang, M.: An analysis of parameterization interactions and sensitivity of single-column model simulations to convection schemes in CAM4 and CAM5, J. Geophys. Res.-Atmos., 118, 8869–8880, https://doi.org/10.1002/jgrd.50690, 2013.

Wang, X., Liu, Y., Zhang, M., Liu, Y., Tang, S., Guo, Z., Wang, K., and Zheng, X.: Evaluation of CAM Single-Column Models in Simulating Convectively Coupled Rossby Gravity Waves During TRMM-KWAJEX, J. Geophys. Res.-Atmos., 131, e2025JD045016, https://doi.org/10.1029/2025JD045016, 2026.

Wang, Y.-C., Pan, H.-L., and Hsu, H.-H.: Impacts of the triggering function of cumulus parameterization on warm-season diurnal rainfall cycles at the Atmospheric Radiation Measurement southern Great Plains site, J. Geophys. Res.-Atmos., 120, 10681–10702, https://doi.org/10.1002/2015JD023337, 2015.

Xie, S. and Zhang, M.: Impact of the convection triggering function on single-column model simulations, J. Geophys. Res.-Atmos., 105, 14983–14996, https://doi.org/10.1029/2000JD900170, 2000.

Xie, S., Wang, Y., Lin, W., Ma, H., Tang, Q., Tang, S., Zheng, X., Golaz, J., Zhang, G. J., and Zhang, M.: Improved diurnal cycle of precipitation in E3SM with a revised convective triggering function, J. Adv. Model. Earth Sy., 11, 2290–2310, https://doi.org/10.1029/2019MS001702, 2019.

Yanai, M., Esbensen, S., and Chu, J.-H.: Determination of bulk properties of tropical cloud clusters from large-scale heat and moisture budgets, J. Atmos. Sci., 30, 611–627, https://doi.org/10.1175/1520-0469(1973)030<0611:DOBPOT>2.0.CO;2, 1973.

Yang, B., Zhou, Y., Zhang, Y., Huang, A., Qian, Y., and Zhang, L.: Simulated precipitation diurnal cycles over East Asia using different CAPE-based convective closure schemes in WRF model, Clim. Dynam., 50, 1639–1658, https://doi.org/10.1007/s00382-017-3712-z, 2018.

Zhang, G. J. and McFarlane, N. A.: Sensitivity of climate simulations to the parameterization of cumulus convection in the Canadian Climate Centre General Circulation Model, Atmos. Ocean, 33, 407–446, https://doi.org/10.1080/07055900.1995.9649539, 1995.

Zhang, G. J.: Convective quasi-equilibrium in midlatitude continental environment and its effect on convective parameterization, J. Geophys. Res.-Atmos., 107, 4220, https://doi.org/10.1029/2001JD001005, 2002.

Zhang, Y., Zhang, F., and Sun, J.: Comparison of the diurnal variations of warm-season precipitation for East Asia vs. North America downstream of the Tibetan Plateau vs. the Rocky Mountains, Atmos. Chem. Phys., 14, 10741–10759, https://doi.org/10.5194/acp-14-10741-2014, 2014.